H_∞ Control of Active Constrained Layer Damping

JOHN L. CRASSIDIS
Catholic University of America
Department of Mechanical Engineering
Washington, D.C. 20064
Member ASME

AMR BAZ
University of Maryland,
Department of Mechanical Engineering
College Park, MD 20742
Fellow ASME

NORMAN WERELEY
University of Maryland,
Department of Aerospace Engineering
College Park, MD 20742
Member ASME

Abstract:

Conventional passive constrained layer damping treatments with visco-elastic cores are provided with built-in sensing and actuation capabilities to actively control and enhance their vibration damping characteristics. Two configurations of the resulting hybrid treatment are considered in this paper. In the first configuration the active control and passive operate separately; whereas in the second configuration, the two operate in unison in order to maximize the energy dissipation characteristics. In this study, three objectives are accomplished. The first objective aims at the design and implementation of robust H_∞ controllers for the separated and unified control strategies. In the second, the performance of the H_∞ controllers at different operating frequencies and temperatures is compared with that of a conventional proportional/derivative controller in order to demonstrate robustness. Finally, a control effort study involving the H_∞ controllers for the separated and unified control strategies is shown in order to assess the efficiency of the active control scheme in controlling structural vibration. The results obtained emphasize the potential of the optimally design unified control strategy as an effective means for providing broad-band attenuation capabilities over a wide range of operating temperatures.

KEY WORDS *Robust H_∞ Control*
Passive Constrained Layer Damping (PCLD)
Active Control/PCLD (AC/PCLD)
Active Constrained Layer Damping (ACLD)

INTRODUCTION

Active Constrained Layer Damping (ACLD) treatments have been successfully utilized as effective means for damping out the vibration of various flexible structures (Agnes and Napolitano, 1993; Azvine et. al., 1994; Baz, 1996-1998; Baz and Ro, 1993-1995; Edberg and Bicos, 1992; Plump and Hubbard, 1986; Shen, 1993; and Van Nostrand et. al., 1994). Such effectiveness is attributed to the high energy dissipation characteristics of the ACLD treatments as compared to conventional constrained damping layers (Baz, 1997-1998 and Chen and Baz, 1996). Furthermore, the ACLD treatments combine the simplicity and reliability of passive damping with the low weight and high efficiency of active controls to attain high damping characteristics over broad frequency bands. These characteristics are particularly suitable for suppressing the vibration of critical systems where damping-to-weight ratio is very important.

The effectiveness of the ACLD treatments is validated experimentally and theoretically using simple proportional and/or derivative (PD) feedback of the transverse deflection or the slope of the deflection line of the base structure. The control gains have generally been selected arbitrarily to be small enough to avoid instability problems, computed based on the stability bounds developed by Shen (1994) for full ACLD treatments or determined using the optimal control strategies devised by Baz and Ro (1995) and Liao and Wang (1995) for partial and full ACLD treatments. In all these attempts, no effort has been exerted to accommodate the uncertainties of the ACLD parameters, particularly those of the visco-elastic cores which arise from the variation of the operating temperature and frequency. Also, in all these studies the controllers are designed without any provisions for rejecting the effects that the external disturbances have on the ACLD/beam system. Only recently, Baz (1998) has theoretically developed a robust H_2 controller to control the ACLD treatments in the presence of parameter uncertainty and external disturbances. The small gain theory is used to guide the selection of the controller gain in order to ensure system stability. The robust H_2 controller is shown to perform successfully over a wide operating temperature and frequency ranges. It has also outperformed the conventional PD controller, which was found to have limited stability margins in the presence

of parameter uncertainty and external disturbances.

In the present study, the work of Baz (1998) is extended to include the theoretical design and experimental evaluation of robust H_∞ controllers which are used to control the operation of surface treatments. The controllers are selected to guarantee stability of the treatments in the presence of parametric uncertainties which may result from variation of the properties of the visco-elastic core of the treatments due to its operation over wide temperature and frequency ranges. At the same time, the selected controllers ensure that the disturbance rejection capabilities of the treatments are maximized over a desired frequency band.

It is important here to note that in the present study, the emphasis is placed on comparing the damping characteristics of beams controlled with the ACLD treatments with those of beams controlled with Active Control (AC) and conventional Passive Constrained Layer Damping (PCLD) treatments. Such an attempt is essential to quantifying the individual contribution of the active and passive damping components, to the overall damping characteristics, when each operates separately as in the case of the AC/PCLD treatments and when both are combined to interact in unison as in the ACLD treatments. In this manner, the selection between AC/PCLD versus ACLD treatments can be based on rational basis. In this study, these rational procedures are based on experimentally validated models which describe the dynamics of beams controlled with AC and PCLD as well as beams treated with ACLD treatments.

To achieve such objectives finite element models and transfer functions are developed to describe the dynamics of beams which are fully-treated with the ACLD and AC/PCLD treatments. The theoretically developed transfer functions of the treatments are validated experimentally using the Eigensystem Realization Algorithm (ERA) (Juang, 1994). The transfer functions are then used to find a robust H_∞ controller (Dorato et. al., 1995; Crassidis et. al., 1994; Dahleh and Diaz-Bobillo, 1995; and Boyd and Barratt, 1991). The controller is selected to minimize the H_∞-norm of the transfer functions between the external disturbances and the deflections at critical locations along the structure to guarantee optimal disturbance rejection capabilities.

The paper is organized as follows. First, the concepts of the ACLD and the AC/PCLD are presented. Then, the finite element models and the transfer functions of the ACLD and

AC/PCLD are developed. Next, the robust H_∞ controller is devised. The performance characteristics of the ACLD with the robust H_∞ controller are then presented in comparison with that of the AC/PCLD. Comparisons are also presented when simple PD controllers are used. Finally, a brief summary of the conclusions is given.

ACLD AND AC/PCLD TREATMENTS

The ACLD treatment consists of a conventional passive constrained layer damping which is augmented with efficient active control means to control the strain of the constrained layer in response to the structural vibrations, as shown in Figure 1a. The visco-elastic damping layer is sandwiched between two piezo-electric layers. The three-layer composite ACLD when bonded to the beam acts as a smart constraining layer damping treatment with built-in sensing and actuation capabilities. The sensing, as indicated by the sensor voltage V_s, is provided by the piezo-electric layer which is directly bonded to the beam surface. The actuation is generated by the other piezo-electric layer which acts as an active constraining layer that is activated by the control voltage V_c. With appropriate strain control, through proper manipulation of V_s, the shear deformation of the visco-elastic damping layer can be increased, the energy dissipation mechanism can be enhanced and the structural vibration can be damped out (Baz, 1996).

As for the AC/PCLD treatment, a typical arrangement is shown in Figure 1b. In this arrangement, a conventional PCLD treatment is formed by sandwiching a visco-elastic layer between two piezo-electric layers. The first piezo-layer, which is bonded to the vibrating beam, acts as a sensor whereas the second piezo-layer is inactive and acts as a passive constraining layer. An additional piezo-layer is bonded to the other side of the beam to actively control its vibration. This layer is activated by a control voltage V_c which is generated by feeding back the sensor control voltage V_s. In this manner, the PCLD and the AC components operate separately.

It is important to note here that the ACLD provides a practical means for controlling the vibration of massive structures with the currently available piezo-electric actuators without the need for excessively large actuation voltages. This is due to the fact that the ACLD properly utilizes the piezo-electric actuator to control the shear in the soft visco-elastic core which is a task compatible with the low-control authority capabilities of the currently available piezo-electric materials. Such desirable characteristics are generally not possible to achieve with the

AC/PCLD treatments as its low-control authority AC component has to operate directly on the vibrating structure. This limits its applicability to relatively soft structures.

THEORETICAL MODELING

In this section, finite element models are outlined, which describe the behavior of Bernoulli-Euler beams with ACLD and AC/PCLD treatments. The models extend the studies of Trompette et. al, (1978) and Rao, (1976) which have been used to analyze the dynamics of passive constrained layer damping. Details of the models are presented in the work of Baz and Ro (1995). The models account for the behavior of the distributed piezo-electric sensor (Miller and Hubbard, 1987) and the distributed piezo-electric actuator (Crawley and de Luis, 1987).

Figure 2 shows a schematic drawing of the ACLD and AC/PCLD treatments of a sandwiched beam which is divided into N finite elements. It is assumed that the shear strains in the piezo-sensor/actuator layers and in the base beam are negligible. The transverse displacements of all points on any cross section of the sandwiched beam are considered to be equal. Furthermore, the piezo-sensor/actuator layers and the base beam are assumed to be elastic and dissipate no energy whereas the core is assumed to be linearly visco-elastic. In addition, the piezo-sensor, the piezo-actuator of the AC/PCLD treatment and the base beam are considered to be perfectly bonded together such that they can be reduced to a single equivalent layer. Accordingly, the original five-layer sandwiched beam reduces to an equivalent three-layer beam.

Degrees of Freedom and Shape Functions

The treated beam elements considered are one-dimensional elements bounded by two nodal points. Each node has four degrees of freedom to describe the longitudinal displacement u_1 of the constraining layer, the longitudinal displacement u_3 of the base beam, the transverse deflection w, and the slope w' of the deflection line. Primes are used to denote spatial derivatives.

The spatial distributions of the longitudinal displacements u_1 and u_3 as well as the transverse deflection w, over any element i of the treated beam, are assumed to be given by

$$u_1 = a_1 x + a_2, u_2 = a_3 x + a_4, \text{ and } w = a_5 x^3 + a_6 x^2 + a_7 x + a_8 \quad (1)$$

where the constants $\{a_1, a_2, \ldots, a_8\}^T = \{\underline{a}\}$ are determined in terms of the eight components of the nodal deflection vector $\{\underline{\Delta}_i\}$ of the *i*th element which is bounded between nodes *j* and *k*. The nodal deflection vector $\{\underline{\Delta}_i\}$ is given by

$$\{\underline{\Delta}_i\} = \{u_{1j}, u_{3j}, w_j, w'_j, u_{1k}, u_{3k}, w_k, w'_k\}^T \tag{2}$$

Therefore, the deflection $\{\underline{\Delta}\} = \{u_1, u_3, w, w'\}^T$ at any location X along the *i*th element can be determined from

$$\{u_1, u_3, w, w'\}^T = \{[\underline{N}_1], [\underline{N}_2], [\underline{N}_3], [\underline{N}_4]\}^T \{\underline{\Delta}_i\} \tag{3}$$

where $[\underline{N}_1]$, $[\underline{N}_2]$, $[\underline{N}_3]$, and $[\underline{N}_4]$ are the spatial interpolating vectors corresponding to u_1, u_3, w, and w', respectively.

Potential and Kinetic Energies

The potential energy U of the beam/treatment system is given by

$$U = \frac{1}{2} \int_{L_i} \left(\sum_{j=1}^{3} E_j A_j u_j'^2 + \sum_{j=1}^{3} E_j I_j w_j''^2 + G_2 A_2 \gamma^2 \right) dx \tag{4}$$

where $E_j A_j$ and $E_j I_j$ are the longitudinal and flexural rigidity of the *j*th layer. Also G_2 and γ are the shear modulus and strain of the visco-elastic core, respectively.

The kinetic energy T of the beam/treatment system is given by

$$T = \frac{1}{2} \int_{L_i} \left(\sum_{j=1}^{3} \rho_j A_j u_j^2 + \sum_{j=1}^{3} E_j I_j w_j^2 \right) dx \tag{5}$$

where ρ_j is the density of the *j*th layer.

Equations of Motion

The dynamics of the ACLD-treated and the AC/PCLD-treated beam element is obtained by applying Hamilton's principle (Meirovitch, 1967)

$$\int_{t_1}^{t_2} \delta(T - U + W)\, dt = 0 \tag{6}$$

where $\delta(\cdot)$ denotes the first variation, and t_1 and t_2 denote initial and final time. Also W denotes the work done by the piezo-electric actuators. This yields the following equation of motion

$$[M_i]\{\ddot{\underline{\Delta}}_i\} + [K_i]\{\underline{\Delta}_i\} = \{\underline{F}_c\} \tag{7}$$

where $[M_i]$ and $[K_i]$ denote the mass and stiffness matrices of the treated beam element. The vector $\{\underline{F}_c\}$ is the vector of control forces and moments generated by the piezo-constraining layer on the treated beam element. It is expressed by

$$\{\underline{F}_c\} = \{F_{p1j}, F_{p3j}, 0, M_{pj}, F_{p1k}, F_{p3k}, 0, M_{pk}\}^T \tag{8}$$

where F_{p1j}, F_{p3j}, F_{p1k}, F_{p3k}, M_{pj}, and M_{pk} denote the control forces and moments generated at nodes *j* and *k*, which are given by

For ACLD Treatments:

$$F_{p1j} = -F_{p1k} = -K_c\, w_e,\ F_{p3j} = -F_{p3k} = 0, \text{ and } M_{pj} = -M_{pk} = -K_c\, D_1\, w_e \tag{9}$$

For AC/PCLD Treatments:

$$F_{p1j} = -F_{p1k} = 0,\ F_{p3j} = -F_{p3k} = -K_c\, w_e, \text{ and } M_{pj} = -M_{pk} = -K_c\, D_2\, w_e \tag{10}$$

where D_1 and D_2 denote the distances between the piezo-constraining layer, the bottom piezo-actuator and the neutral axis of the beam as shown in Figure 2. Also, K_c denotes the transfer function of the control gains.

Equation (7) describes the dynamics/control of a single treated beam element. Assembly of the corresponding equations for the different elements and applying the proper boundary conditions yields the overall equation for the entire treated beam system, as given by the following equation

$$[M_o]\{\ddot{\underline{\Delta}}\} + [K_o]\{\underline{\Delta}\} = \{\underline{F}_{co}\} \tag{11}$$

where $[M_o]$ and $[K_o]$ denote the overall mass and stiffness matrices, respectively. Also $\{\underline{\Delta}\}$ and $\{\underline{F}_{co}\}$ denote the overall nodal deflection and control vectors, respectively. The resulting equation is then utilized as a basis for comparing the damping characteristics of beams treated with the ACLD and AC/PCLD treatments.

Transfer Function

The transfer function approach has been utilized recently to study the stability of ACLD treatments with certain parameters (Shen, 1994). The approach has also been adopted in 1986 by Alberts et. al. to define the stability limits for rotating beams treated with PCLD of fixed parameters. In the present study, the transfer function approach is employed to design the controller of the ACLD and AC/PCLD treatment, in order to ensure stability in the presence of parameter uncertainty and guarantee optimal disturbance rejection capabilities. Equation (11) is used to extract the transfer functions of the ACLD and AC/PCLD as follows

$$\{\underline{X}\}/\{\underline{F}_{co}\} = G(s) = C(sI - A)^{-1}B \tag{12}$$

where A, B, and C are the state-space matrices representing equation (11). Also, $\{\underline{X}\}$ is the state variables vector $\left\{\underline{\Delta}^T, \dot{\underline{\Delta}}^T\right\}^T$, and $G(s)$ is the system transfer function in the Laplace s domain.

DEVELOPMENT OF THE ROBUST CONTROLLER

Overview

Figure 3 shows a block diagram of a robust controller with transfer function F that stabilizes the ACLD/beam system with transfer function G in the presence of parameter uncertainty when the system is subjected to external disturbance. The H_∞ control strategy, as compared to classical control techniques, provides advanced methods and perspectives for designing control systems. This is accomplished by shaping the frequency response characteristics of a plant according to pre-specified performance specifications in the form of frequency dependent weighting functions. The principal advantages of the H_∞ control strategy include: (i) it supplies robust stability to structural uncertainties, (ii) it achieves performance requirements efficiently, (iii) it handles both disturbance and excessive control authority problems easily, and (iv) it not only works on single-input-single-output (SISO) systems, but also on multi-input-multi-output (MIMO) systems.

Therefore, frequency response criteria can easily be shaped to desired specifications. Some of the disadvantages the H_∞ control strategy include: (i) large controller dimensions, (ii) the limited applicability to time-invariant systems, and (iii) choosing weighting functions properly. However, for vibration suppression of time-invariant systems, the advantages of using an H_∞ controller make it a desirable strategy (in particular, due to the inherent robustness feature).

Vibration Suppression

The loop-shaping approach (Maciejowski, 1989) shows a clear tradeoff between performance and robustness of a multivariable system. However, this methodology does not enable a practical design approach for active damping, since plant dynamics are usually canceled by compensator dynamics. This section expands upon the fundamental H_∞ control formulation in order to provide a means of incorporating active damping into a structure with inherently low structural damping (Crassidis et. al., 1994).

In order to achieve damping, the block diagram in Figure 4 is used. Let the MIMO plant $G(s)$ be partitioned into "disturbance" $G_1(s)$ and "plant/actuator" $G_2(s)$ transfer functions, so that

$$Y_2(s) = G_1(s)U_{1a}(s) + G_2(s)U_2(s) \tag{13}$$

The inputs in Figure 4 are: $U_{1a}(s)$, any disturbance into the structure, and $U_{1b}(s)$, a fictitious input used to simulate sensor uncertainty. The controller is represented by $F(s)$, and $U_2(s)$ and $Y_2(s)$ represent the system input and output, respectively. The "augmented" plant with control compensator is now represented by Figure 5, where W_1, W_2, and W_3 are appropriately selected weighting functions.

The open-loop transfer function matrix of the augmented plant now becomes

$$\begin{bmatrix} Y_{1a} \\ Y_{1b} \\ Y_{1c} \\ -- \\ Y_2 \end{bmatrix} = \left[\begin{array}{cc|c} W_1 G_1 & W_1 & -W_1 G_2 \\ 0 & 0 & W_2 \\ 0 & 0 & W_3 G_2 \\ -- & -- & -- \\ G_1 & I & -G_2 \end{array}\right] \begin{bmatrix} U_{1a} \\ U_{1b} \\ -- \\ U_2 \end{bmatrix} \tag{14}$$

where U_2 and Y_2 are the controller output and input, respectively. The sensitivity function between the disturbance input and plant output now becomes

$$S(s) = \frac{G_1}{I + F\,G_2} \tag{15}$$

Therefore, active damping is now accomplished since pole locations of the closed-loop transfer function in equation (15) are shifted by the controller F and plant/actuator transfer functions. From Figure 5, the characteristics of the weighting function $W_1(s)$ determine the amount of damping and frequency response dynamics of the closed-loop system. The complementary sensitivity (sensor uncertainty) function is weighted by $W_3(s)$, and controller/limiter function is weighted by $W_2(s)$. Once the augmented plant in equation (14) is formed, the two-Riccati algorithm for the computation of the H_∞ controller can be used (Doyle et. al., 1989). The MIMO state-space representation of the augmented plant in Equation (14) now becomes

$$\begin{bmatrix} \dot{\underline{x}}_g \\ \dot{\underline{x}}_{w1} \\ \dot{\underline{x}}_{w2} \\ \dot{\underline{x}}_{w3} \end{bmatrix} = \begin{bmatrix} A_g & 0 & 0 & 0 \\ B_{w_1}C_g & A_{w_1} & 0 & 0 \\ 0 & 0 & A_{w_2} & 0 \\ B_{w_3}C_g & 0 & 0 & A_{w_3} \end{bmatrix} \begin{bmatrix} \underline{x}_g \\ \underline{x}_{w1} \\ \underline{x}_{w2} \\ \underline{x}_{w3} \end{bmatrix} + \left[\begin{array}{cc:c} B_{g_1} & 0 & -B_{g_2} \\ B_{w_1}D_{g_1} & B_{w_1} & -B_{w_1}D_{g_2} \\ 0 & 0 & B_{w_2} \\ 0 & 0 & B_{w_3}D_{g_2} \end{array}\right] \begin{bmatrix} u_{1a} \\ \underline{u_{1b}} \\ \underline{u_2} \end{bmatrix} \tag{16}$$

with output given by

$$\left[\begin{array}{c} y_{1a} \\ y_{1b} \\ \underline{y_{1c}} \\ y_2 \end{array}\right] = \left[\begin{array}{cccc} D_{w_1}C_g & C_{w_1} & 0 & 0 \\ 0 & 0 & C_{w_2} & 0 \\ D_{w_3}C_g & 0 & 0 & C_{w_3} \\ \hdashline C_g & 0 & 0 & 0 \end{array}\right] \begin{bmatrix} \underline{x}_g \\ \underline{x}_{w1} \\ \underline{x}_{w2} \\ \underline{x}_{w3} \end{bmatrix} + \left[\begin{array}{cc:c} D_{w_1}D_{g_1} & D_{w_1} & -D_{w_1}D_{g_2} \\ 0 & 0 & D_{w_2} \\ 0 & 0 & D_{w_3}D_{g_2} \\ \hdashline D_{g_1} & I & -D_{g_2} \end{array}\right] \begin{bmatrix} u_{1a} \\ \underline{u_{1b}} \\ \underline{u_2} \end{bmatrix} \tag{17}$$

PERFORMANCE WITH ACLD AND AC/PCLD TREATMENTS

In this section, the experimental performance characteristics of beams treated with ACLD treatments are determined and compared with those treated with the AC/PCLD treatments at different operating temperature and frequency. The comparisons presented include the vibration, damping characteristics, and control voltages, as well as comparisons between the theoretical predictions and experimental measurements.

Properties of Base Beam, Visco-Elastic and Constraining Layers

Table 1 lists the main physical, geometrical, and dynamical properties of the base beam. The beam is made of aluminum and is mounted in a cantilevered configuration. The first natural frequency of the untreated test beam is 7.02 Hz and the corresponding modal damping ratio is 0.0173, as determined experimentally using classical modal analysis techniques.

Table 1 - Main Properties of the Base Beam

Length ($L-m$)	Width ($b-m$)	Thickness (h_3-cm)	Density (kg/m^3)	Young's Modulus (GN/m^2)	First Mode Freq.	Damp.
0.263	0.0492	0.0813	2700	70.2	7 Hz	1.73%

The beam treatment of the ACLD and AC/PCLD consists of a visco-elastic sheet of DYAD-606 from SOUNDCOAT sandwiched between two piezo-electric layers from AMP, Inc. (Valley Forge, PA). The piezo-electric layers are made from PVDF polymeric films number S028NAO. Table 2 lists the physical and geometrical parameters of the visco-elastic and piezo-electric layers. Under open-loop conditions, the experimental first natural frequency of the fully-treated test beam becomes 6.76 Hz, and the corresponding modal damping ratio is 0.022.

Table 2 - Physical and Geometrical Properties of the ACLD and PCLD Treatments

Layer	Length (m)	Width (m)	Thickness (m)	Density (kg/m^3)	Modulus (Mpa)
Viscoelastic	0.263	0.0492	0.0005	1104	20*
Piezoelectric	0.263	0.0492	$28x10^{-6}$	1800	2250**

** Young's modulus * shear modulus

The shear modulus and loss factor of the visco-elastic material used in this study are shown in Figures 6a and 6b, respectively, at different operating temperatures and frequencies. The figures demonstrate clearly that the complex modulus of the visco-elastic core varies dramatically, when the operating temperature is varied from 20° C to 50° C, and the frequency is scanned over a 100Hz-bandwidth. Such pronounced changes in the properties of the visco-elastic layer introduce significant uncertainties in the parameters of the ACLD and AC/PCLD treatments. Figure 7 shows the theoretical transfer functions of beams treated with the ACLD and AC/PCLD. The displayed transfer functions relate the transverse displacement w_e of the free end of the beam to the inputs to the piezo-electric actuators at 20° C to 50° C. Five beam elements are used to compute the transfer functions with a total of 16 degrees of freedom.

EXPERIMENTAL SET-UP

Figure 8 shows a schematic drawing of the experimental set-up used to compare the performance of the effectiveness of the ACLD and the AC/PCLD in attenuating the vibration of the test beam. The test beam is excited by an electro-mechanical speaker driven by a sinusoidal or white noise source through a power amplifier. The amplitude of vibration of the free end of the beam is monitored by a laser sensor (Model MQ - Aeromat Corp., Providence, NJ). The output signal of the sensor is sent to a spectrum analyzer to determine the vibration attenuation both in the time and frequency domains. The laser sensor has accuracy of 20 μm over a frequency band between 0-1000 Hz.

The sensor signal is sampled at a rate of 0.005 s using a dSPACE input-output system, which includes a DS1002 33Mhz processor board, DS2002 32 channel A/D board, and DS2101 5 channel D/A board. The signal is manipulated using either the robust H_∞ control law or the conventional PD control law. The resulting control action is sent via an analog power amplifier (Model PA7C from Wilcoxon Research, Rockville, MD) to either the piezo-electric constraining layer in the case of the ACLD treatment or the bottom piezo-electric actuator in the case of the AC treatment.

EXPERIMENTAL RESULTS

In this section, the experimental results using a PD and an H_∞ control law for the ACLD and AC/PCLD systems are shown. First, the identification method and open-loop characteristics of each system are summarized. Then, the design approach for each control law and system is shown. Finally, the performance and robustness of each controller are tested in order to access the validity of the design approaches with analytical comparisons.

Open-Loop Characteristics of the ACLD/Beam System

A state model is required to perform an optimal control design. The Eigensystem Realization Algorithm (ERA) provides a viable approach for determining MIMO models from experimental data. The test beam is excited using random inputs at the speaker and control input locations. The random response and input data is then converted to impulse response data, which is used in ERA to identify a state-space-model. Figure 9 shows the open-loop (i.e., from the speaker excitation to the laser sensor output) transfer-function magnitude plots for the AC/PCLD and ACLD systems. It is clearly seen that the first mode is at about 7 Hz, which agrees with the

theoretical analysis. Also, the magnitude difference between the AC/PCLD and ACLD at the first mode is about 20 dB, which also agrees with theoretical prediction. The second mode of the test beam is at about 47 Hz, which is significantly more damped than the first mode.

Robust Control Design

In this section, the concepts and limitations for the selection of the proper weighting functions used in the H_∞ design are presented. The appropriate selection of the weighting functions over the desired frequency range is not explicitly related to the performance objectives in a straightforward manner. Numerous trial weighting functions are usually required in order to obtain desired performance objectives.

The goal of the H_∞ design is to reshape the open-loop dynamics in order to provide vibration suppression in the frequency region considered. The W_1 (sensitivity) weighting function is used to reshape the desired frequency characteristics to provide adequate damping in the test beam. The W_3 weighting function is used as an uncertainty weight for the sensor output. Since the laser sensor is extremely accurate, this weighting function was not deemed to be critical; therefore, it was omitted in the initial control design. The W_2 weighting function is used to shape the control response characteristics. The overall controller is derived by incorporating all weighting functions and open-loop models into the augmented system shown by equations (16) and (17).

The H_∞ design is used to target the first model of the test beam. A plot of the inverse W_1 and W_2 weighting functions is shown in Figure 10. The W_1^{-1} function weights the sensitivity function along the zero dB region over the desired target frequency. The W_2^{-1} function is used to obtain an attenuated controller response at both lower and higher frequencies. This results in a third-order weighting functions that simulates a band-pass filter. The choice of this weighting function insures that the controller does not destabilize higher frequency modes, and also attenuates control signals at lower frequencies.

The selection of these weighting functions provides adequate damping in the closed-loop system. An optimal H_∞ controller solution, using the γ iteration technique (Doyle et. al., 1989) can be determined. The order of the subsequent controller is 13, which is effectively reduced to a 2nd-order controller using the Schur balanced model reduction method (Safanov and Chiang, 1988). The PD control gains chosen to provide adequate damping performance in the first mode

of the test beam. A plot of the H_∞ and PD control magnitudes for the ACLD system is shown in Figure 11. A plot of the simulated damping responses using the two controllers is shown in Figure 12. Clearly, both controllers are able to attenuate the first mode of the test beam. Also, the second mode becomes less damped using the PD controller, as compared to the open-loop response. This may be due to spillover effects from the high frequency amplification of the PD controller.

Control Results

In this section, results using the H_∞ and PD controllers are shown for the actual test beam. Two sets of test cases are presented. The first set involves using the controllers on the AC/PCLD and ACLD systems at room temperature (20° C). The second case involves the controllers on both systems at a temperature of 50° C. As shown previously, such pronounced temperature changes introduce significant uncertainties in the parameters of the ACLD and AC/PCLD treatments.

The H_∞ and PD controllers are designed to damp the first mode of the test beam using the room temperature model only. Sensitivity to uncertainties can be investigated by applying small gain theory to the closed-loop system. This is accomplished by using a sufficiency test for stability robustness with a multiplicative uncertainty (Crassidis et. al., 1994), given by

$$\overline{\sigma}\left[\Delta_m(s)\right] < \frac{1}{\overline{\sigma}\left\{F(s)\left[I + G(s)\,F(s)\right]\right\}^{-1}} \tag{18}$$

where $\Delta_m(s)$ denotes multiplicative uncertainties and $\overline{\sigma}$ denotes the maximum singular value over the desired frequency region. A plot of the theoretical uncertainty bound, using the right hand side of equation (18), for the ACLD system at room temperature using the H_∞ and PD controllers is shown in Figure 13. Although the PD controller is well-known for providing damping in a system due to phase margin enhancement, Figure 13 indicates that the PD controller is susceptible to uncertainties in the first mode.

A plot of the actual controlled responses for the ACLD system at room temperature is shown in Figure 14. Damping has been increased by more than of factor of two for both controllers. This shows excellent agreement with design results in Figure 12 for both modes. A plot of the controlled responses for the AC/PCLD system at room temperature is shown in Figure 15. These

results have been achieved after numerous trial parameter tuning of the PD gains. For this case the H_∞ controller outperforms the PD controller. This may be due to the fact that the AC/PCLD system requires a higher DC gain than the ACLD case, which the simple PD controller cannot provide without amplifying higher modes. The next test case involves both systems and controllers at the higher temperature (50° C). Plots of the ACLD and AC/PCLD systems for this case are shown in Figures 16 and 17. Clearly, the H_∞ controller provides robustness over a wide variation in visco-elastic property changes. The PD controller provides robustness in the second mode, but lacks robustness in the first mode, which agrees with theoretical predictions in Figure 13. In fact the PD controlled response is even *worse* than the open-loop response for the AC/PCLD case, while the H_∞ controller remains at the original damping performance. Therefore, the study clearly indicates that the H_∞ control scheme provides an effective means for damping out structural vibrations for both systems over a wide temperature variation. Finally, the ACLD requires less control effort (about 1/2) than the AC/PCLD system. This is shown by applying an impulse input of 1 mVolt into the H_∞ controller for both the ACLD and AC/PCLD. The control output for both cases is shown in Figure 18. Therefore, since active control effort is less, the ACLD system provides a more effective means for broad-band attenuation as compared to the AC/PCLD system.

CONCLUSIONS

This paper has presented a theoretical and experimental comparisons between the damping characteristics of beams treated with ACLD and AC/PCLD treatments. In these comparisons the individual contribution of the active and passive damping components, to the overall damping characteristics, is quantified when these two components operate separately as in the AC/PCLD treatments, and when both are combined to interact in unison as in the ACLD treatments. The comparisons are based on experimentally validated finite element models which are developed to describe the dynamics of beams controlled with AC/PCLD as well as beams treated with ACLD treatments.

These models are used to derive expressions for the transfer functions of the beam/treatment systems and devise a robust H_∞ control strategy which is stable in the presence of parameter uncertainty. Furthermore, the developed control strategy also insures optimal disturbance rejection capabilities. Experimental results are presented to demonstrate the effectiveness of the

robust controller in damping out structural vibrations when the ACLD and AC/PCLD treatments operate over wide temperature and frequency ranges. Under similar operating circumstances, it is found that a simple PD controller fails to produce any significant vibration control when the stability constraints are imposed over the entire range of operation.

Finally, it is important to note that the ACLD treatment is found to be more effective in damping the structural vibration than the AC/PCLD treatment. It requires less control effort in the presence of external disturbances and parameter uncertainty.

Acknowledgments: *This work is funded by the U.S. Army Research Office (Grant number DAAH-04-96-0317). Special thanks are due to Dr. Gary Anderson, the technical monitor, for his invaluable technical inputs.*

REFERENCES

1. Alberts, T., Dickerson, S., and Book, W., 1986, "On the Transfer Function Modeling of Flexible Structures With Distributed Damping," in *Robotics: Theory and Applications, ASME*, New York, 23-30.

2. Agnes, G. S. and Napolitano, K., 1993, "Active Constrained Layer Viscoelastic Damping," in *Proceedings of 34th SDM Conference*, April, 3499-3506.

3. Azvine, B., Tomlinson G. and Wynne, R., 1994, "Initial Studies into the Use of Active Constrained-Layer Damping for Controlling Resonant Vibrations," in *Proceedings of Smart Structures and Materials Conference on Passive Damping*, ed. C. Johnson, Vol. 2193, Orlando, Florida, 138-149.

4. Bailey, T. and Hubbard, J., 1985, "Distributed Piezo-electric Polymer Active Vibration Control of a Cantilever Beam," *Journal of Guidance and Control*, Vol. 8, 606-611.

5. Baz, A., 1996, "Active Constrained Layer Damping," U.S. Patent #5,485,053.

6. Baz, A., 1997, "Boundary Control of Beams Using Active Constrained Layer Damping," *ASME Journal of Vibration and Acoustics*, Vol. 199, 166-172.

7. Baz, A., 1998, "Robust Control of Active Constrained Layer Damping," *Journal of Sound and Vibration*, Vol. 221, No. 3, pp.467-480.

8. Baz, A. and Ro, J., 1993, "Partial Treatment of Flexible Beams with Active Constrained

Layer Damping," *Conference of Engineering Sciences Society*, ASME-AMD-Vol. 167, pp. 61-80, Charlottesville, VA, June, 61-80.

9. Baz, A. and Ro, J., 1994, "Actively-Controlled Constrained Layer Damping," *Sound & Vibration Magazine*, Vol. 28, No. 3, 18-21.
10. Baz, A. and Ro, J., 1995, "Optimum Design and Control of Active Constrained Layer Damping," *ASME Journal of Vibration and Acoustics*, Vol. 117 B, 135-144.
11. Boyd, S. and Barratt, C., 1991, *Linear Controller Design: Limits of Performance*, Prentice Hall, Englewood Cliffs, NJ.
12. Butkovskiy, A.G., *Distributed Control Systems*, 1969, American Elsevier Publishing Co., Inc., New York.
13. Chen, T. and Baz, A., 1996, "Performance Characteristics of Active Control with Passive Constrained Layer Damping versus Active Constrained Layer Damping," *Conference on Smart Materials and Structures*, San Diego, CA.
14. Crawley, E. and DeLuis, J., 1987, "Use of Piezoelectric Actuators as Elements in Intelligent Structures," *J. of AIAA*, Vol. 25, No. 10, 1373-1385.
15. Crassidis, J.L., Leo, D.J., Inman, D.J., and Mook, D.J., 1994, "Robust Identification and Vibration Suppression of a Flexible Structure," *Journal of Guidance, Control, and Dynamics*, Vol. 17, No. 5, 921-928.
16. Dahleh, M. and Diaz-Bobillo, I., 1995, *Control of Uncertain Systems: A Linear Programming Approach*, Prentice Hall, Englewood Cliffs, NJ.
17. Dorato, P., Abdallah C., and Cerone, V., 1995, *Linear Quadratic Control: An Introduction*, Prentice Hall, Englewood Cliffs, NJ.
18. Dosch, J.J., Inman, D.J., and Garcia, E., 1992, "A Self-Sensing Piezoelectric Actuator for Collocated Control," *J. of Intelligent Material Systems and Structures*, Vol. 3, 166-184.
19. Douglas, B.E. and Yang, J., 1978,"Transverse Compressional Damping in the Vibratory Response of Elastic-Viscoelastic-Elastic Beams," *AIAA Journal*, Vol. 16, No. 9, 925-930.
20. Doyle, J.C., Glover, K., Khargonekar, P.P., and Francis, B.A., 1989,"State-Space Solutions

of Standard H_2 and H_∞ Control Problems," *IEEE Transactions on Automatic Control*, Vol. AC-29, 831-847.

21. Edberg, D. and Bicos, A., 1992, "Design and Development of Passive and Active Damping Concepts for Adaptive Structures," *Conference on Active Materials and Adaptive Structures*, ed. by G. Knowles, IOP Publishing Ltd., Bristol, UK, 377-382.

22. Juang, R. N., *Applied System Identification*, 1994, Prentice Hall, Englewood Cliffs, NJ.

23. Lam, M.J., Saunders, W.R., and Inman, D.J., 1995, "Modeling Active Constrained Layer Damping using Finite Element Analysis and GHM Damping Approach," *Smart Structures and Materials Conference*, Paper number 2445-09, San Diego, CA, March.

24. Liao, W. and Wang, K., 1995, "On the Active-Passive Hybrid Vibration Control Actions of Structures with Active Constrained Layer Damping," *ASME Design Engineering Technical Conference*, Boston, MA, DE-Vol. 84-3, 125-141.

25. Maciejowski, J.M., *Multivariable Feedback Design*, 1989, Addison-Wesley Pub. Co., Wokingham, England.

26. Mead, D.J. and Markus, S., 1969, "The Forced Vibration of a Three-Layer, Damped Sandwich Beam with Arbitrary Boundary Conditions," *Journal of Sound and Vibration*, Vol. 10, No. 1, 163-175.

27. Meirovitch, L., *Analytical Methods in Vibrations*, 1967, MacMillan Pub. Co., Inc., New York.

28. Miller, S. and Hubbard, Jr., J., 1987, "Observability of a Bernoulli-Euler Beam using PVF2 as a Distributed Sensor," *7th Conference on Dynamics & Control of Large Structures*, VPI & SU, Blacksburg, VA, May, 375-930.

29. Nashif, A., Jones, D.I., and Henderson, J.P., 1985, *Vibration Damping*, J. Wiley & Sons, New York.

30. Plump, J. and Hubbard, J.E., 1986, "Modeling of An Active Constrained Layer Damper," *Twelve International Congress on Acoustics*, Paper # D41, Toronto, Canada, 24-31.

31. Rao, D.K., 1976, "Static Response of Stiffed-Cored Unsymmetric Sandwich Beams," *ASME*

Journal of Engineering for Industry, Vol. 98, 391-396.

32. Safonov, M.G., and Chiang, R.Y., 1988, "A Schur Method for Balanced Model Reduction," in *Proceedings of the American Control Conference*, Atlanta, GA.

33. Shen, I.Y., 1994, "Hybrid Damping Through Intelligent Constrained Layer Treatments," *ASME Journal of Vibration and Acoustics*, Vol. 116, No. 3, 341-349.

34. Trompette, P., Boillot, D., and Ravanel, M.A., 1978, "The Effect of Boundary Conditions on the Vibration of a Viscoelastically Damped Cantilever Beam," *Journal of Sound and Vibration*, Vol. 60, No. 3, 345-350.

35. Van Nostrand, W., Knowles, G., and Inman, D.J., 1994, "Finite Element Modeling for Active Constrained-Layer Damping," in *Proceedings of Smart Structures and Materials Conference on Passive Damping*, ed. C. Johnson, Vol. 2193, Orlando, Florida, 126- 137.

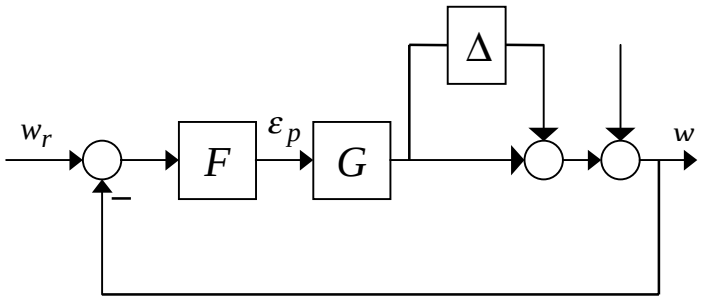
Δ
w_r
ε_p
F
G
w
−

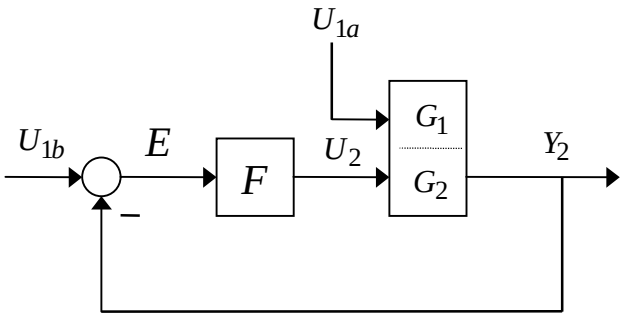
U_{1a}
G_1
U_{1b}
E
F
U_2
G_2
Y_2
−

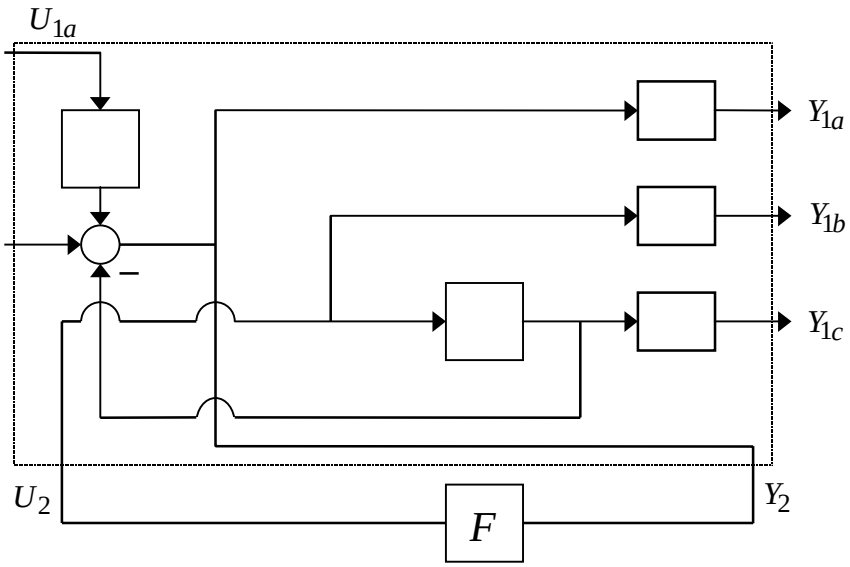
U_{1a}
Y_{1a}
Y_{1b}
Y_{1c}
−
U_2
F
Y_2

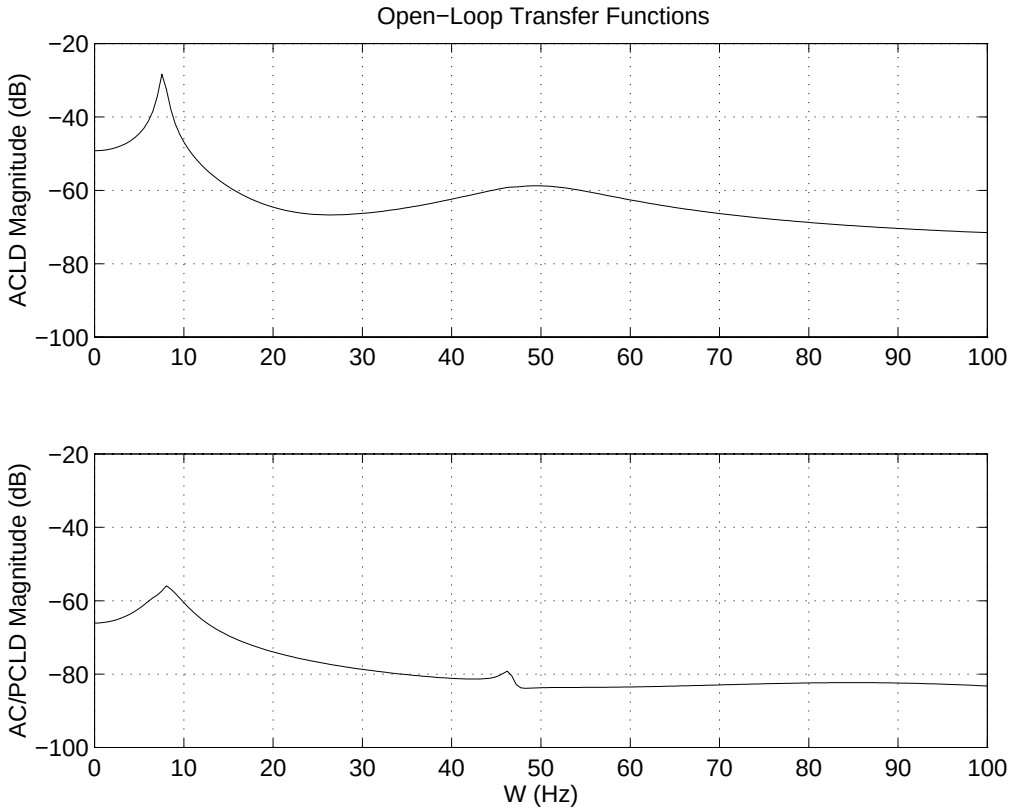
Open−Loop Transfer Functions
ACLD Magnitude (dB)
−20
−40
−60
−80
−100
0
10
20
30
40
50
60
70
80
90
100
AC/PCLD Magnitude (dB)
−20
−40
−60
−80
−100
0
10
20
30
40
50
60
70
80
90
100
W (Hz)

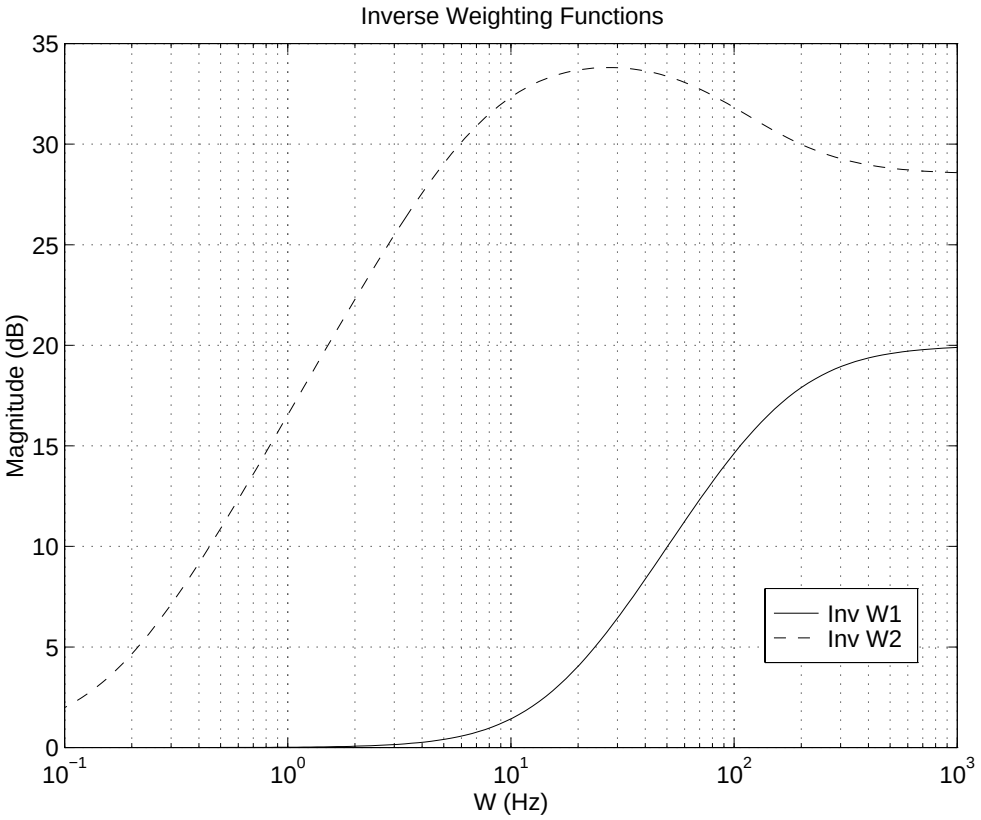
Inverse Weighting Functions
Magnitude (dB)
W (Hz)
Inv W1
Inv W2
35
30
25
20
15
10
5
0
10^{-1}
10^{0}
10^{1}
10^{2}
10^{3}

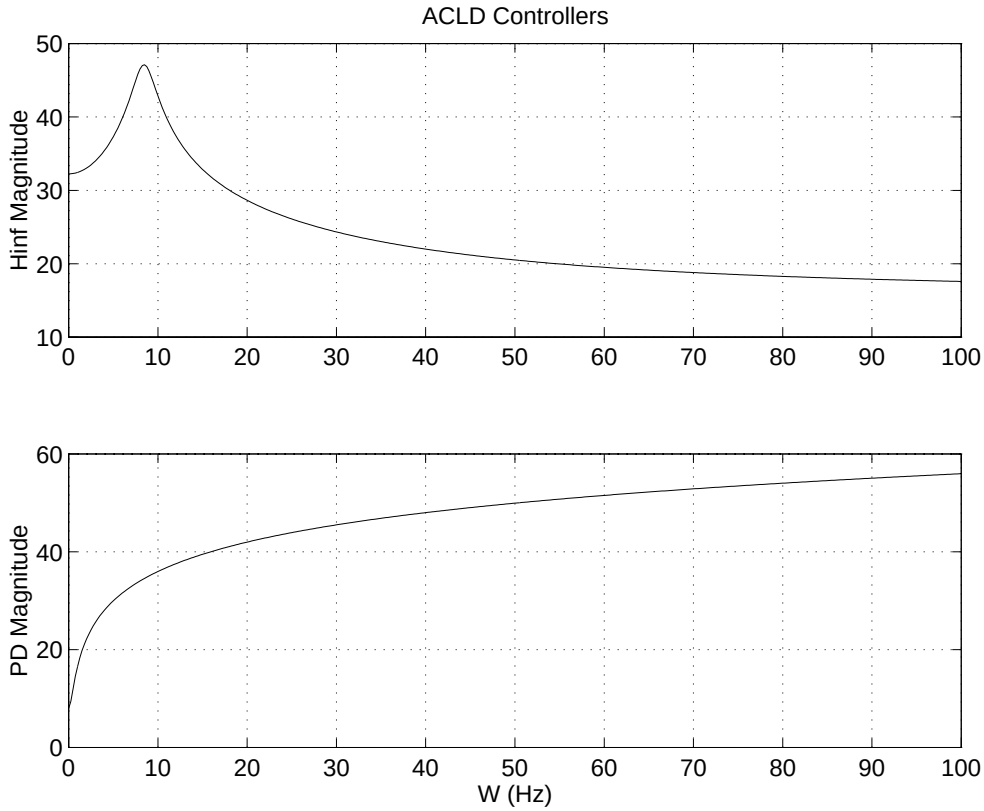
ACLD Controllers
Hinf Magnitude
PD Magnitude
W (Hz)
50
40
30
20
10
60
0
10
20
30
40
50
60
70
80
90
100

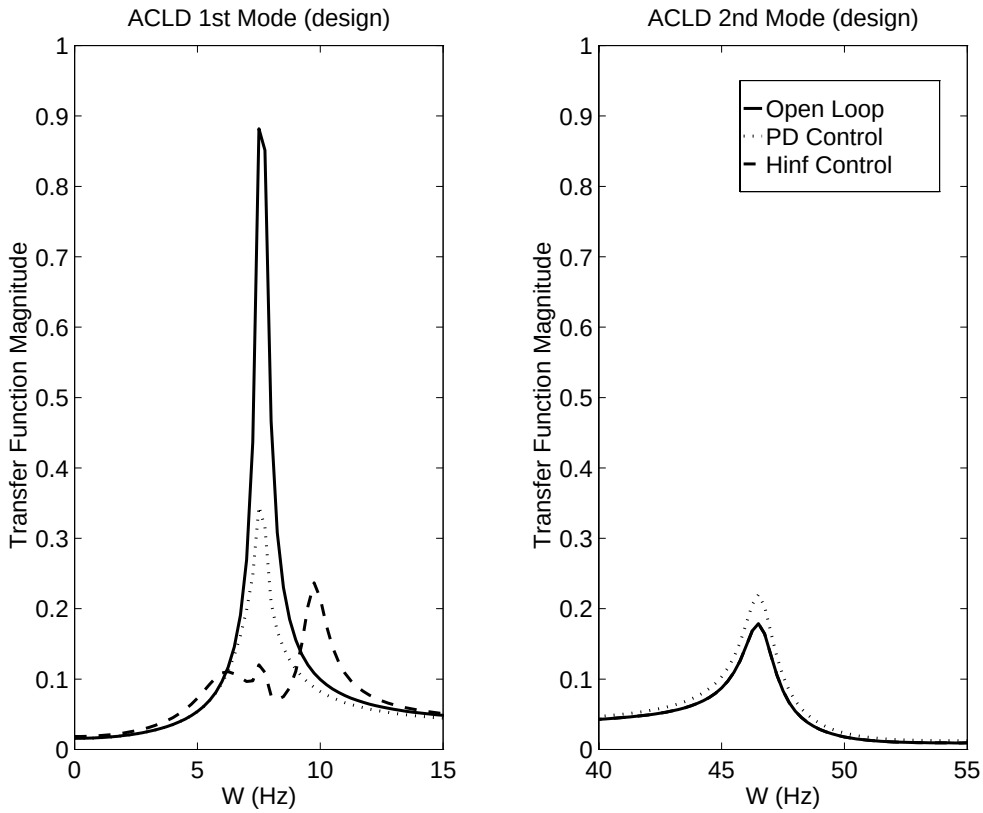
ACLD 1st Mode (design)
Transfer Function Magnitude
W (Hz)
0
0.1
0.2
0.3
0.4
0.5
0.6
0.7
0.8
0.9
1
0
5
10
15
ACLD 2nd Mode (design)
Transfer Function Magnitude
W (Hz)
Open Loop
PD Control
Hinf Control
40
45
50
55

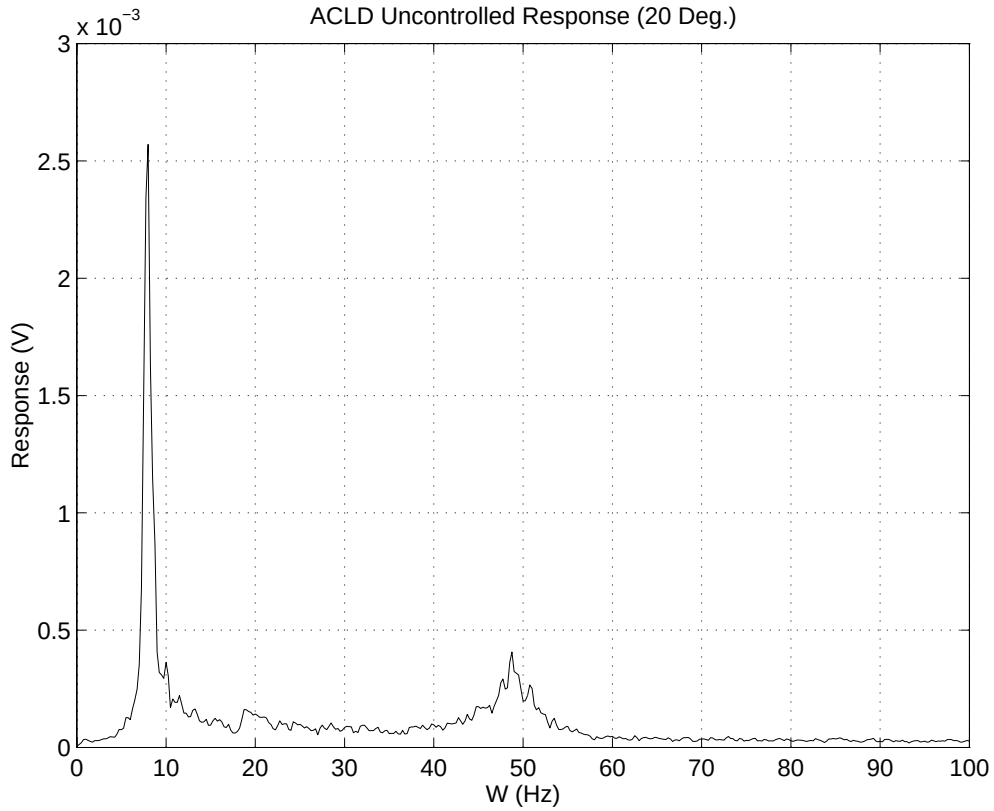
ACLD Uncontrolled Response (20 Deg.)
x 10^−3
Response (V)
W (Hz)
0
0.5
1
1.5
2
2.5
3
0
10
20
30
40
50
60
70
80
90
100

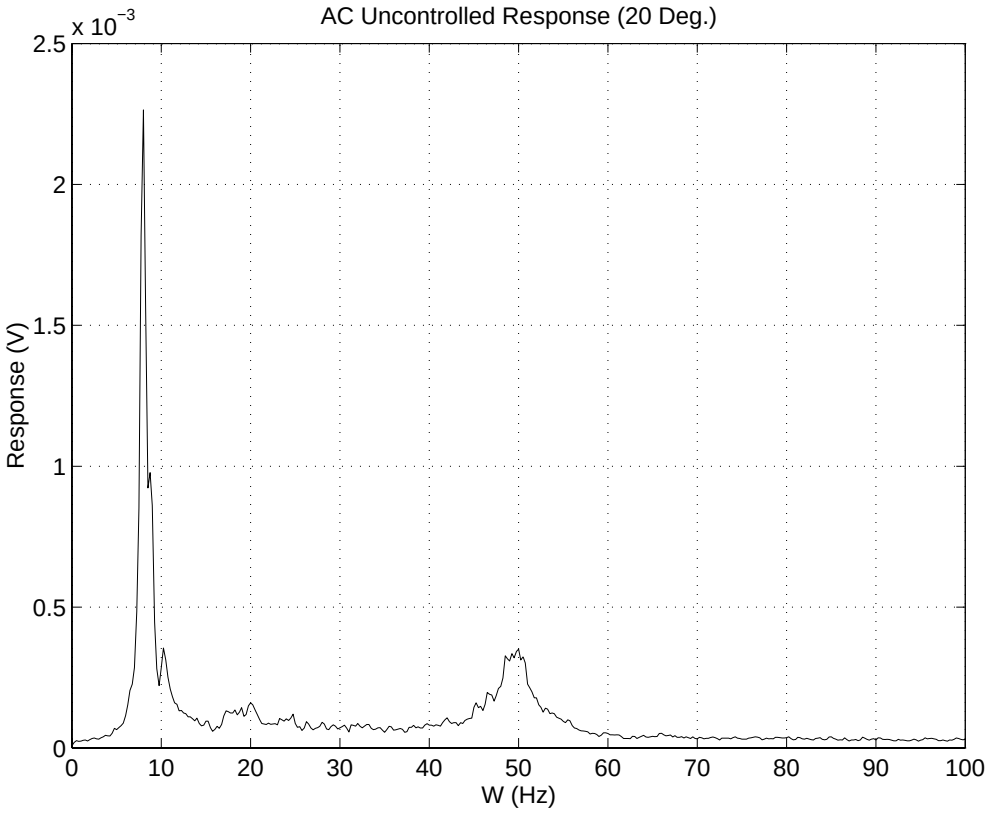
AC Uncontrolled Response (20 Deg.)
x 10^−3
Response (V)
W (Hz)
0
0.5
1
1.5
2
2.5
0
10
20
30
40
50
60
70
80
90
100

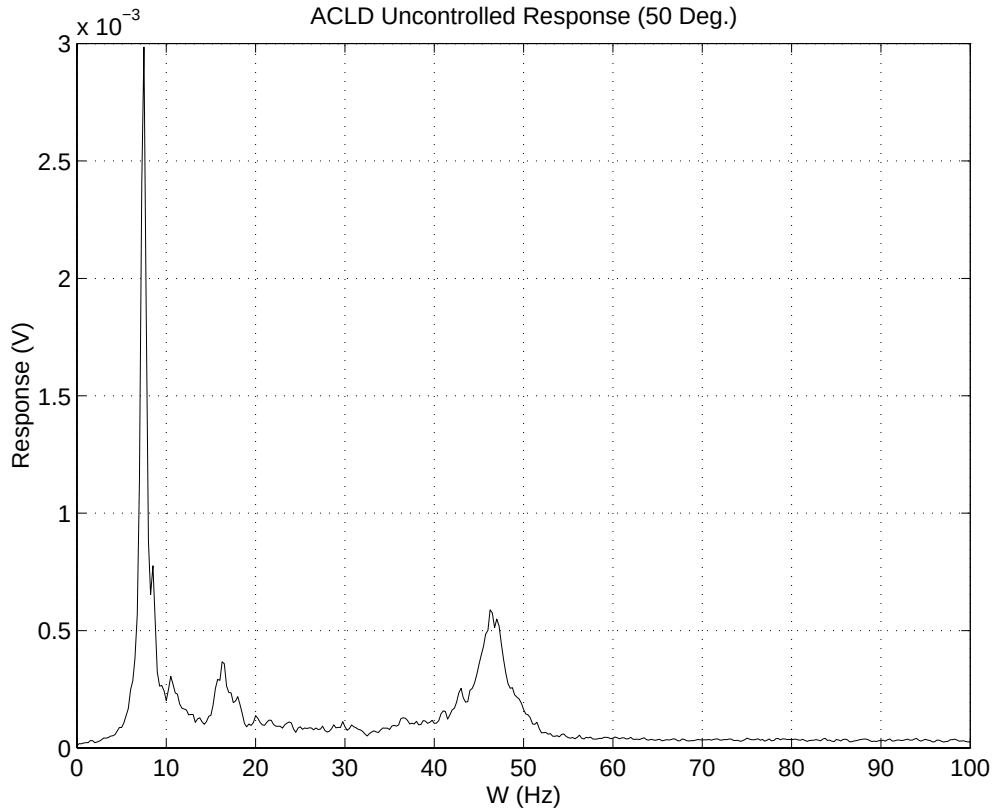
ACLD Uncontrolled Response (50 Deg.)
x 10^−3
Response (V)
W (Hz)
0
0.5
1
1.5
2
2.5
3
0
10
20
30
40
50
60
70
80
90
100

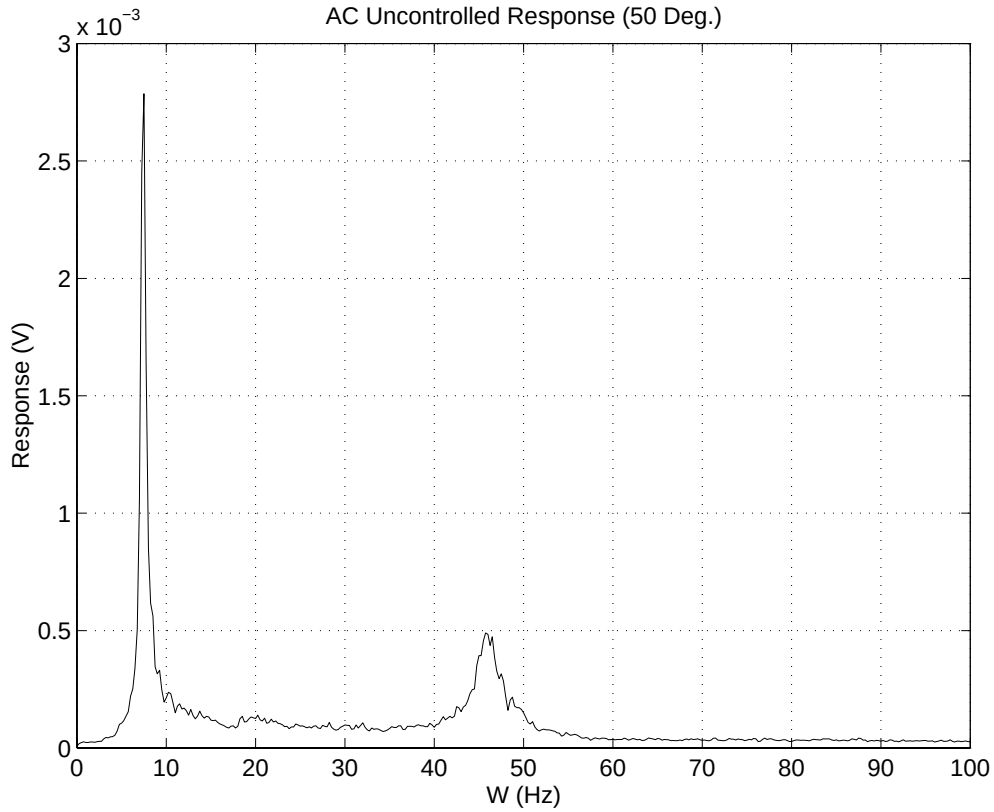
AC Uncontrolled Response (50 Deg.)
x 10^−3
Response (V)
W (Hz)
0
0.5
1
1.5
2
2.5
3
0
10
20
30
40
50
60
70
80
90
100

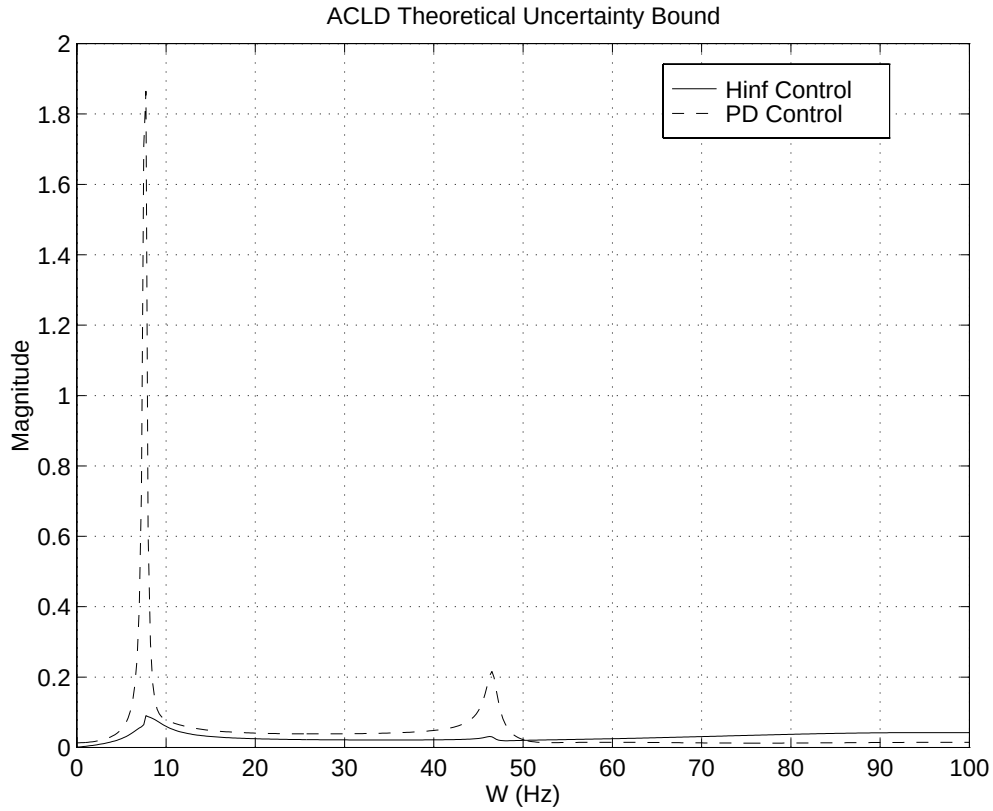
ACLD Theoretical Uncertainty Bound
Hinf Control
PD Control
Magnitude
W (Hz)
0
0.2
0.4
0.6
0.8
1
1.2
1.4
1.6
1.8
2
0
10
20
30
40
50
60
70
80
90
100

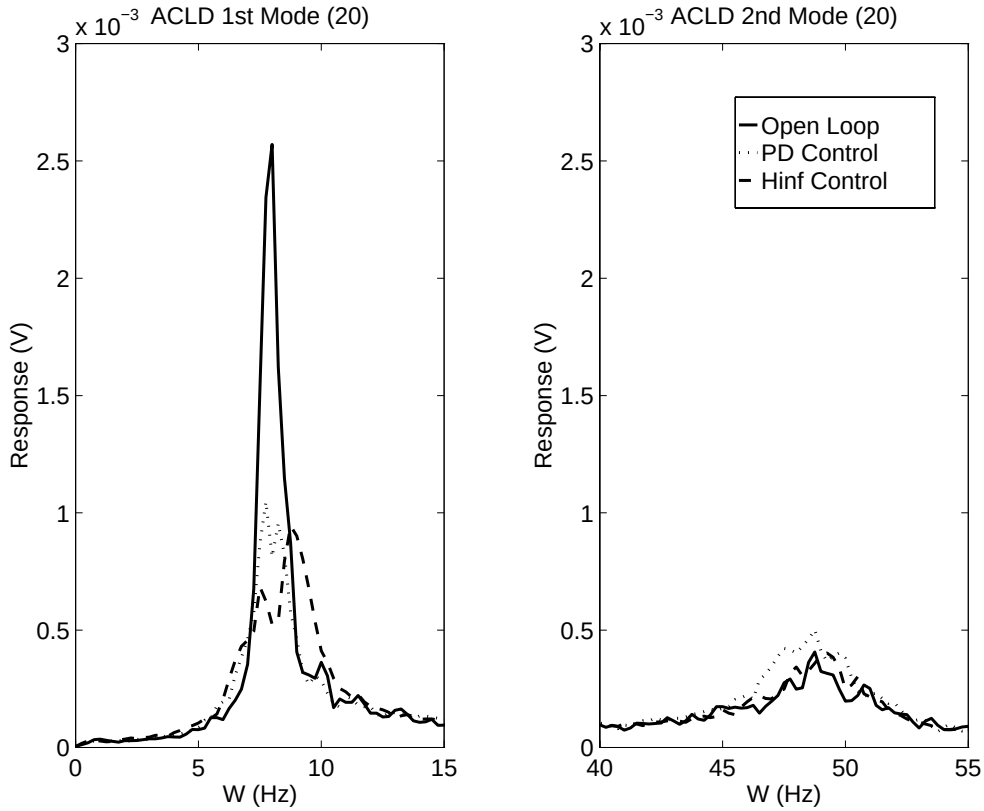
x 10^−3 ACLD 1st Mode (20)
Response (V)
W (Hz)
0
0.5
1
1.5
2
2.5
3
0
5
10
15
x 10^−3 ACLD 2nd Mode (20)
Response (V)
W (Hz)
40
45
50
55
Open Loop
PD Control
Hinf Control

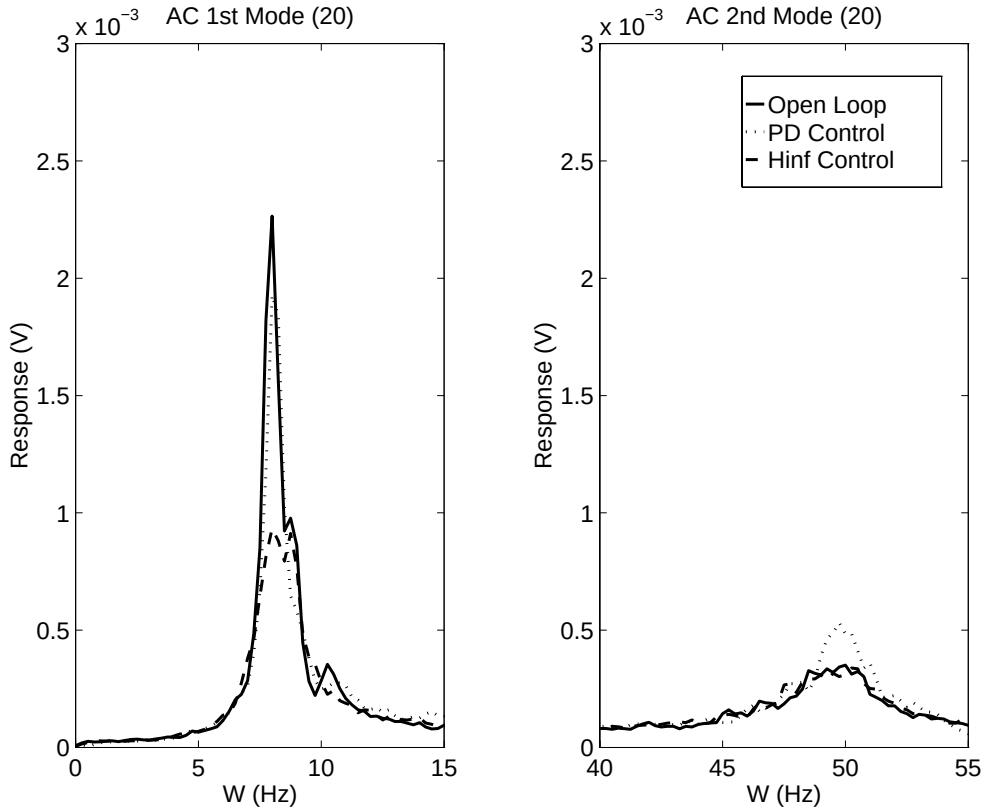
x 10^−3
AC 1st Mode (20)
Response (V)
W (Hz)
0
0.5
1
1.5
2
2.5
3
0
5
10
15
x 10^−3
AC 2nd Mode (20)
Response (V)
W (Hz)
40
45
50
55
Open Loop
PD Control
Hinf Control

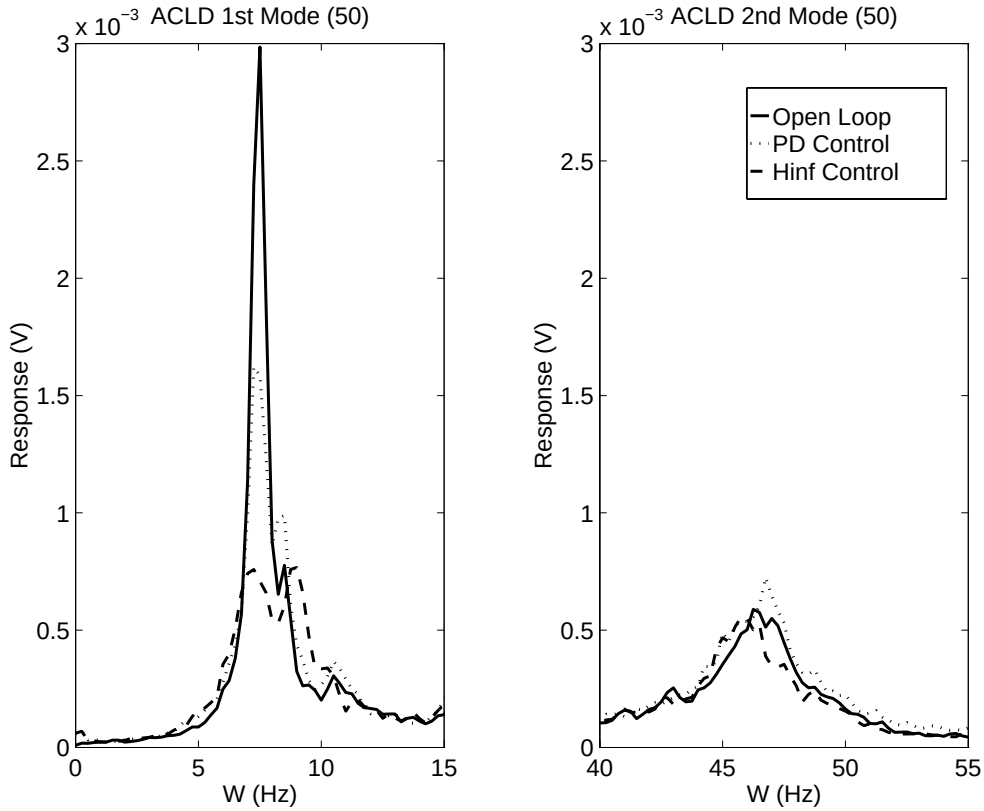
x 10^−3 ACLD 1st Mode (50)
Response (V)
W (Hz)
0
0.5
1
1.5
2
2.5
3
0
5
10
15
x 10^−3 ACLD 2nd Mode (50)
Response (V)
W (Hz)
40
45
50
55
Open Loop
PD Control
Hinf Control

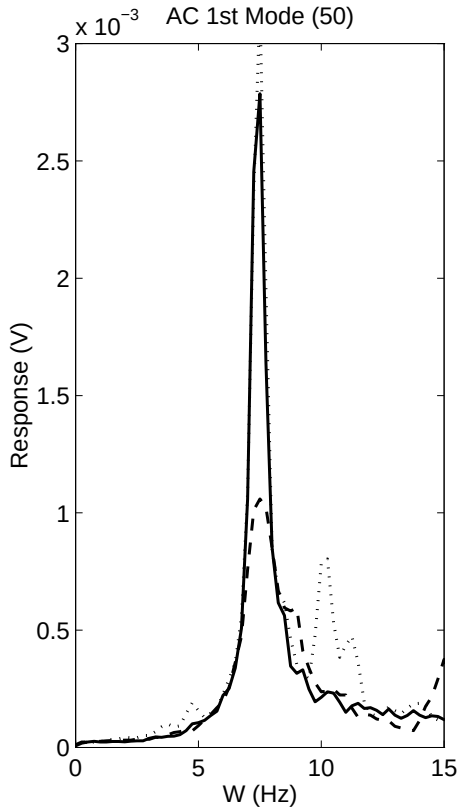
x 10^−3
AC 1st Mode (50)
Response (V)
W (Hz)
0
0.5
1
1.5
2
2.5
3
0
5
10
15

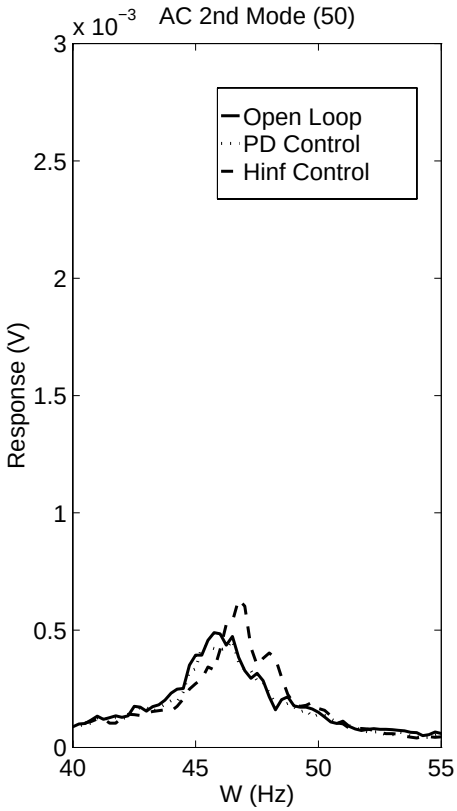
x 10^−3
AC 2nd Mode (50)
Response (V)
W (Hz)
Open Loop
PD Control
Hinf Control
0
0.5
1
1.5
2
2.5
3
40
45
50
55

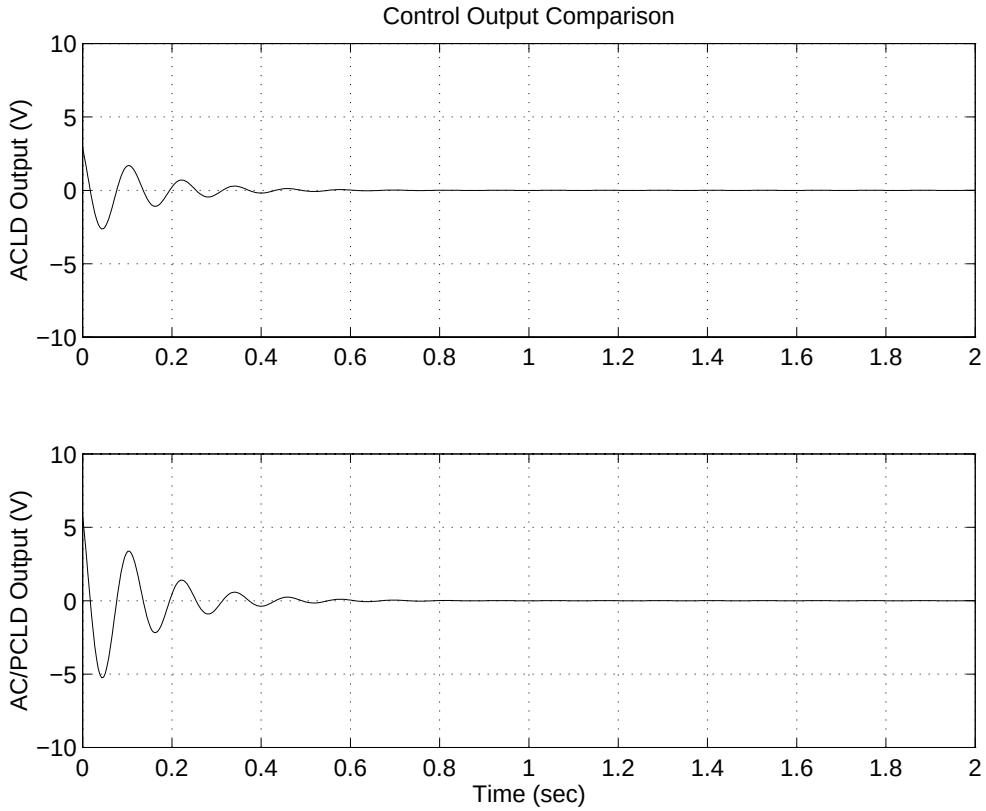
Control Output Comparison
ACLD Output (V)
AC/PCLD Output (V)
Time (sec)
10
5
0
−5
−10
0
0.2
0.4
0.6
0.8
1
1.2
1.4
1.6
1.8
2